

Research article

A Small Molecule Tubulin Depolymerizing Agent Identified by a Phenotypic Drug Discovery Approach

Carla Ríos-Luci¹, Elena Díaz-Rodríguez², Rubén M. Buey³, Inês J. Sousa⁴, Miguel X. Fernandes^{1,4}, Atanasio Pandiella², José M. Padrón^{1,*}

¹Instituto Universitario de Bio-Orgánica "Antonio González" (IUBO-AG), Centro de Investigaciones Biomédicas de Canarias (CIBICAN), Universidad de La Laguna, C/ Astrofísico Francisco Sánchez 2, 38206 La Laguna, Spain

²Instituto de Biología Molecular y Celular del Cáncer, Campus Miguel de Unamuno, 37007 Salamanca, Spain

³Metabolic Engineering Group, Dept. Microbiology and Genetics, Universidad de Salamanca, Campus Miguel de Unamuno, 37007 Salamanca, Spain

⁴Centro de Química da Madeira, Universidade da Madeira, Campus da Penteadá, 9000-390 Funchal, Portugal

*Correspondence: jmpadron@ull.es (José M. Padrón)

<https://doi.org/10.31083/j.jmcm.2018.02.003>

Abstract

In the scenario of drug discovery, numerous *in vitro* testing initiatives had been established. Thus far, no general methodology is reputable and literature on this hot topic is scarce. In this respect, we propose a strategy based on a Phenotypic Drug Discovery approach. Within our program directed at the discovery of new antitumor agents, we have focused our attention on compounds that disturb the cell cycle. Our strategy relies on the use of a set of biological assays organized in a modular fashion. Herein, we exemplified this strategy with a family of propargylic enol ether derivatives. Using different assays in sequential stages and in a stepwise manner, our studies allowed us to understand the bioactivity of this family of compounds and led us to identify tubulin as the main molecular target.

Keywords

Anti-cancer; Colchicine binding site; Drug-target interaction; Microtubule-targeting agents; Tubulin-depolymerizing agents

Submitted: November 3, 2017; Accepted: December 8, 2017

1. Introduction

The development of new anti-neoplastic drugs remains a key to advance novel cancer treatments. Nowadays, it is widely accepted that in the discovery of new biologically active compounds, it is essential to use suitable screening methodologies that can address the mechanism of action, at early stages of drug discovery. In addition, identifying the correct target of new bioactive molecules is critical to prevent further drug development failures. In the scenario of drug discovery, numerous *in vitro* testing initiatives had been established with variable degrees of success.

To date, there is no universal systematic process to discover the cellular target or mode of action for any given compound [1]. As a result of this approach, we have previously reported on a new family of small molecule catalytic inhibitors of human DNA topoisomerase II alpha (TOP2) [2]. The lead compound, named DTA0100, was selected for further biological evaluation. Further studies suggested that their anti-proliferative activity is not chiral-dependent and docking studies reinforced that they act as catalytic inhibitors of the nuclear enzyme TOP2 [3]. In a recent study, DTA0100 was tagged with dansyl to generate fluorescently-labeled DTA0100 (dns-DTA0100). In this study, besides inhibition of TOP2, DTA0100 was found to act as a microtubule-targeting agent whose pharmacokinetics were not changed in the presence of P-glycoprotein (P-gp) [4].

The results from the aforementioned investigations forced us to re-evaluate the cellular targets of DTA0100. Regardless of the outcome of these experiments, it was clear that DTA0100 affected the mitotic machinery. Herein we report on the effects caused by

DTA0100 in relation to perturbations in the cell cycle, induction of apoptosis, cell signaling pathways and changes in cell morphology.

2. Materials and Methods

2.1. Reagents and immunochemicals

DTA0100 (Methyl 4-((E)-2-(methoxycarbonyl)vinyl)oxy)oct-2-ynoate) was prepared according to the procedure described in the literature [2]. 2-Methoxy-5-(2, 3, 4-trimethoxyphenyl)-2, 4, 6-cycloheptatrien-1-one (MTC), was kindly provided by Dr. José M. Andreu (Centro de Investigaciones Biológicas, CSIC, Madrid, Spain).

Antibodies used in this study included pRb (ser807/811), caspase-3, active-caspase-3, caspase-8, nucleoporin 62 and BubR1 (BD Biosciences, San Jose, CA); γ H2AX (Ser 139), pChk2 (Thr 64), caspase-7 and caspase-9 (Cell Signaling, Danvers, MA); PARP-1, Mcl-1, Bcl-2, cyclin B1, cyclin D1 and GAPDH (Santa Cruz Biotechnology, Santa Cruz, CA); β -tubulin (Sigma, St. Louis, MO) and pH3 (ser 10) (Upstate, Cambridge, MA). Horseradish peroxidase-conjugated secondary antibodies were from Bio-Rad (Hercules, CA) and fluorochrome conjugated ones were from Invitrogen (Carlsbad, CA) and Jackson ImmunoResearch (West Grove, PA).

2.2. Cell lines and cell culture

Non-small human lung cancer cell line SW1573 and its P-gp overexpressing variant (SW1573/Pgp) was kindly provided by Dr. Godefridus J. Peters (Cancer Center Amsterdam, Vrije Universiteit,

Amsterdam, The Netherlands). All cells were grown in DMEM supplemented with 1 mM glutamine, 10% (HBL-100) or 5% (SW1573 and HeLa) FBS and antibiotics. Cells were grown at 37°C in a humidified atmosphere of 5% CO₂ and maintained at low passage.

2.3. TOP2 nuclear extracts from tumor cells and DNA relaxation assay

Nuclear extracts were prepared according to the protocol suggested by TopoGen Inc (Columbus, USA). In brief, exponentially growing cells were scraped off into medium and centrifuged at 800 × g for 3 min. Pellets were resuspended in 3-5 mL of TEMP buffer (10 mM Tris-HCl pH 7.5, 1 mM EDTA, 4 mM MgCl₂, 0.5 mM PMSF) and clumps were dispersed by pipetting up and down. Cells were then centrifuged at 800 × g for 3 min and resuspended in 3 mL of TEMP buffer. Samples were kept on ice for 10 min and centrifuged at 1500 × g for 10 min. After centrifugation, pellets were resuspended in 1 mL of TEMP buffer, and centrifuged at 1500 × g for 10 min. Nuclei pellets were then resuspended in a small volume (no more than 4 pellet volumes) of TEP buffer (same as TEMP buffer but lacking MgCl₂). An equal amount of 1 M NaCl was added, vortexed and the mix was left on ice for 30-60 min. Samples were then centrifuged at 15,000 × g for 20 min. Final supernatants containing TOP2 activity were transferred to new microfuge tubes and stored at -20°C until analysis. All the procedure was carried out at 4°C because this enzyme undergoes rapid inactivation and can undergo rapid proteolysis.

The DNA relaxation assay was performed using the negatively supercoiled pHOT1 plasmid as a DNA substrate. The reaction mixture (20 µL) contained 250 ng of pHOT1 plasmid and 0.5 mM ATP in assay buffer (10 mM Tris-HCl, 50 mM KCl, 50 mM NaCl, 0.1 mM EDTA, 5 mM MgCl₂, and 2.5% [v/v] glycerol, pH 8.0). Chemical compounds were at 100 µM in 0.25% DMSO. The reaction was initiated by the addition of 2 units of TOP2. The samples were incubated at 37°C for 30-60 min, and quenched with 1% (w/v) SDS and 25 mM Na₂EDTA. The mixture was treated with 50 µg/mL proteinase K at 37°C for 30 min. pHOT1 topoisomers were resolved by 1% (w/v) agarose gel electrophoresis in 1 × TBE buffer (89 mM Tris-borate and 2 mM Na₂EDTA, pH 8.0) without ethidium bromide. The photograph was taken after staining with ethidium bromide.

2.4. Cell cycle analysis and mitotic index

Changes in cell cycle distribution and mitotic index determination were assessed by flow cytometry. Briefly, 2-5 × 10⁵ cells were treated with DTA0100 for the indicated time and subsequently collected by pooling together the non-attached and attached cells. After washing with PBS, cells were fixed overnight at -20°C with 70% cold-ethanol. For cell cycle analysis, fixed cells were centrifuged at 1,500 rpm for 10 min. Cell pellets were resuspended in 500 µL of PBS containing 5 µL of DNase-free RNase solution (10 mg/mL). The mixture was incubated at 37°C for 30 min and 5 µL of propidium iodide (PI; 0.5 mg/mL) were added. Then, DNA content analysis was performed. Cells were acquired on a LRSII Flow Cytometer (Becton Dickinson, San José, USA), and the fractions of cells in G₀/G₁, S, and G₂/M phase were calculated using FACS Diva 6.0 software. For each sample, 20,000 events were collected and cell aggregates were gated out.

To estimate the percent of cells that enter mitosis, ethanol-fixed cells were washed twice with PBS (1% BSA) and permeabilized

by PBS containing 1% BSA, 0.25% Triton X-100 for 5 min on ice. After two PBS washes, cells were resuspended in 100 µL PBS (1% BSA) containing anti-phospho histone 3 (1:100) and left incubating for 3 hours at room temperature. Cells were then washed twice and incubated for an additional hour with FITC-conjugated secondary antibody (1: 100) protected from light. Cells were washed as before, and resuspended in 500 µL of PBS (containing 0.5 mg/mL DNase-free RNase and 5 µg/mL PI). PI-stained cells were analyzed by flow cytometry as described above.

2.5. Apoptosis assays

Cells were plated at 0.2-0.5 × 10⁵ cells per well in 6-well plates. The number of apoptotic cells was determined using the FITC Annexin V Apoptosis Detection Kit I (BD Biosciences) according to the manufacturer's protocol. Fluorescence measurements were performed using a LSRII Flow Cytometer (Becton Dickinson). Results were analyzed using FACSdiva (Becton Dickinson) software.

To analyze the effect of DTA0100 on mitochondrial membrane potential, an early marker for apoptosis, the cell-permeant red-orange dye TMRE was used [5]. Cells were stained with 0.5 µM TMRE (Stock 1 mM, DMSO) 30 min before the end of the experiment. After incubation, cells were trypsinized, harvested, transferred to test tubes (12 × 75 mm) and centrifuged at 200 × g for 5 min. Pellets were resuspended in 500 µL of PBS, vortexed and analyzed by flow cytometry. The loss of mitochondrial membrane potential was quantified using tetramethylrhodamine, ethyl ester (TMRE) fluorescence intensity in FL2 channel.

2.6. Western blot analysis

To prepare protein extracts for western blot analysis, cells at 60-70% confluence were treated with DTA0100 for 12, 24, 36 and 48 h. After treatment, cells were washed twice with cold-PBS and lysed in ice-cold lysis buffer freshly supplemented with protease and phosphatase inhibitors (20 mM Tris pH 8.0, 140 mM NaCl, 1% NP-40, 10% glycerol, 5 mM EDTA, 2 mM Na₃VO₄, 10 mM Na₂P₂O₇, 10 mM NaF, 10 µg/mL aprotinin, 10 µg/mL leupeptin, 0.5 µg/mL pepstatin, and 1 mM PMSF). Lysates were incubated on ice for 10 min and then cell debris were spun down at 12,000 rpm for 10 min. After centrifugation, supernatants were transferred to new tubes and stored at -20°C.

Protein concentration was determined by the Bradford method [6]. Equal amounts of protein were resolved by SDS/PAGE and electro-transferred onto PVDF membranes. Membranes were blocked in Tris-buffered saline with Tween (TBST; 100 mM Tris pH 7.5, 150 mM NaCl, 0.05% Tween 20) containing 1% of BSA for 1 h and then incubated with the corresponding primary antibody for 2-16 h. After washing three times with TBST, membranes were incubated with HRP-conjugated secondary antibodies for 30 min, washed three times with TBST and bands were visualized by a luminol-based detection system with p-iodophenol enhancement.

2.7. Indirect immunofluorescence microscopy

For indirect immunofluorescence, cells were cultured on poly-L-lysine coated glass coverslips (22 × 22 mm) and treated with DTA0100 for the indicated times. Then, cells were washed with PBS and fixed in 2% paraformaldehyde (PFA) for 30 min at room temperature. Fixed cells were washed in PBS and quenched in 50 mM NH₄Cl for 10 min, washed again in PBS and permeabilized

in PBS supplemented with 0.1% Triton X-100. After blocking in PBS supplemented with 0.2% BSA, cells were incubated with β -tubulin (1:350) or nucleoporin 62 antibodies (1:400) for at least 1 h at room temperature. Following three washes with blocking solution, monolayers were incubated with Alexa 488 or Alexa 568 conjugated anti-mouse secondary antibodies (1:1000) for 30 min protected from light, washed with PBS and counterstained with 4,6-diamidino-2-phenylindole (DAPI) to stain nuclei. Finally, coverslips were mounted on microscope slides with Gelvatol. Samples were analyzed by confocal immunofluorescence microscopy using a SP5 Leica apparatus with LAS-AF software (Leica Microsystems, Wetzlar, Germany).

2.8. Microtubule polymerization assays

To evaluate the effect of DTA0100 on microtubule polymerization, two different methods were used. For the ultracentrifugation assay, purified tubulin was equilibrated prior to use in pre-chilled PEM buffer (80 mM pipes-KOH, 1 mM EGTA-KOH, 4 mM MgCl₂, 3.4 M [29% v/v] glycerol, pH 6.8). Aggregates were removed by centrifugation at 100,000 × g for 10 min in a TLA120 rotor at 4°C in an Optima TLX centrifuge (Beckman Coulter, Brea, USA). Tubulin was kept on ice and 1 mM GTP (Sigma, the pH of GTP stock was pre-adjusted to 7) was added to stabilize the protein. The solution was distributed in 200 μ L polycarbonate tubes (TLA 120 rotor). The assay was performed in a total reaction volume of 50 μ L, containing 20 μ M of tubulin and compounds at the same concentration. Sample tubes were incubated for 30 min at 37°C. After incubation, samples were centrifuged at 100,000 × g for 10 min at 37°C. The supernatant containing unassembled tubulin was carefully collected and transferred to new microfuge tubes and the microtubule pellets were resuspended in 50 μ L of cold buffer (without GTP) and left on ice for 20 min. The supernatant and pellet fractions were analyzed by SDS-PAGE and protein bands stained with Coomassie.

The microtubule-turbidity assay was carried out using the tubulin polymerization kit (Cytoskeleton Inc, Denver, USA). The assay was performed according to the manufacturer's recommended procedure. In short, each experimental compound (final concentration of 10 μ M) was incubated with GTP-supplemented tubulin supernatant (3 mg/mL) in a 96-well plate at 37°C. Polymerization reactions were followed by absorbance at 340 nm for 30 min every 20 seconds using a BioTek's PowerWave XS Absorbance Microplate Reader.

2.9. Colchicine tubulin-binding assay

Colchicine binding site assay was studied using the colchicine analog MTC (2-methoxy-5-(2',3',4'-trimethoxy)-2,4,6-cycloheptatrien-1-one). Results of the MTC displacement experiments were analyzed using a cell-free fluorescence-based assay. In brief, tubulin was equilibrated previous to use in PG buffer (10 mM sodium phosphate, 1 mM EGTA, 1 mM MgCl₂ and 10 μ M of GTP). Tubulin concentration was determined spectrophotometrically using an extinction coefficient of 1.16 L g⁻¹ cm⁻¹ at 280 nm and adjusting to 10 μ M. Samples were prepared by mixing tubulin with 10 μ M MTC and increasing concentrations of the test drug in PG buffer. All binding measurements were monitored spectrofluorometrically at 25°C, using a Fluoromax-3 (HORIBA Jobin-Yvon, Kyoto, Japan) equipped with a constant temperature water circulating bath. A 1 cm path-length quartz cuvette was used. Fluorescence emission spectra were recorded between 350-600 nm upon excitation at 350 nm (2 nm

slit). Data were acquired with FluorEssence (Horiba Jobin-Yvon) software and plotted using SigmaPlot 11.0 (Systat Software Inc, Chicago, USA).

2.10. Molecular modeling

The crystal structure of the colchicine pocket of α , β -tubulin (PDB ID: 3E22) was utilized as a template for docking studies using the program AutoDock Vina (The Scripps Research Institute, La Jolla, USA). Initial structures were drawn and minimized using AM1 semi-empirical method, with a gradient energy minimization method until the energy change between steps was lower than 0.01 kcal/mol (Hyperchem, Hypercube, USA). The algorithm used was the Polak-Ribiere (conjugate gradient). The best solution (based on docking score) was retained for further analysis. PyMol v1.5 (Shrödinger Inc, Portland, USA) was used for visualization and identification of residues in the binding pocket [7].

2.11. Anti-proliferative activity

Cells were maintained in RPMI-1640 supplemented with glutamine, 5% FBS and antibiotics. The anti-proliferative assays were conducted following our variation of the protocol of the National Cancer Institute [8]. Besides DTA0100, the commercially available microtubule interacting drugs colchicine, vincristine, vinblastine and paclitaxel were used. Verapamil was applied as a P-gp inhibitor.

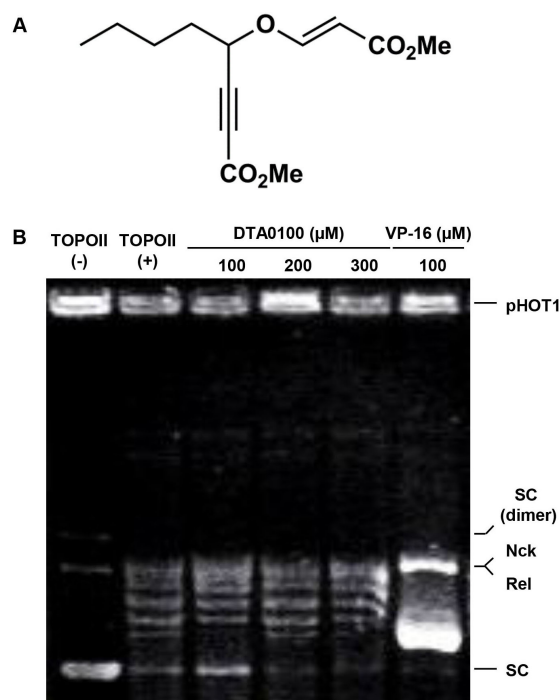


Fig. 1. (A) Chemical structure of DTA0100. (B) DTA0100 did not inhibit TOPO II α activity of SW1573 nuclear extracts. Nuclear preparations were exposed to increasing concentrations of DTA0100 for 1 h, after which the supercoiled relaxation assay was performed.

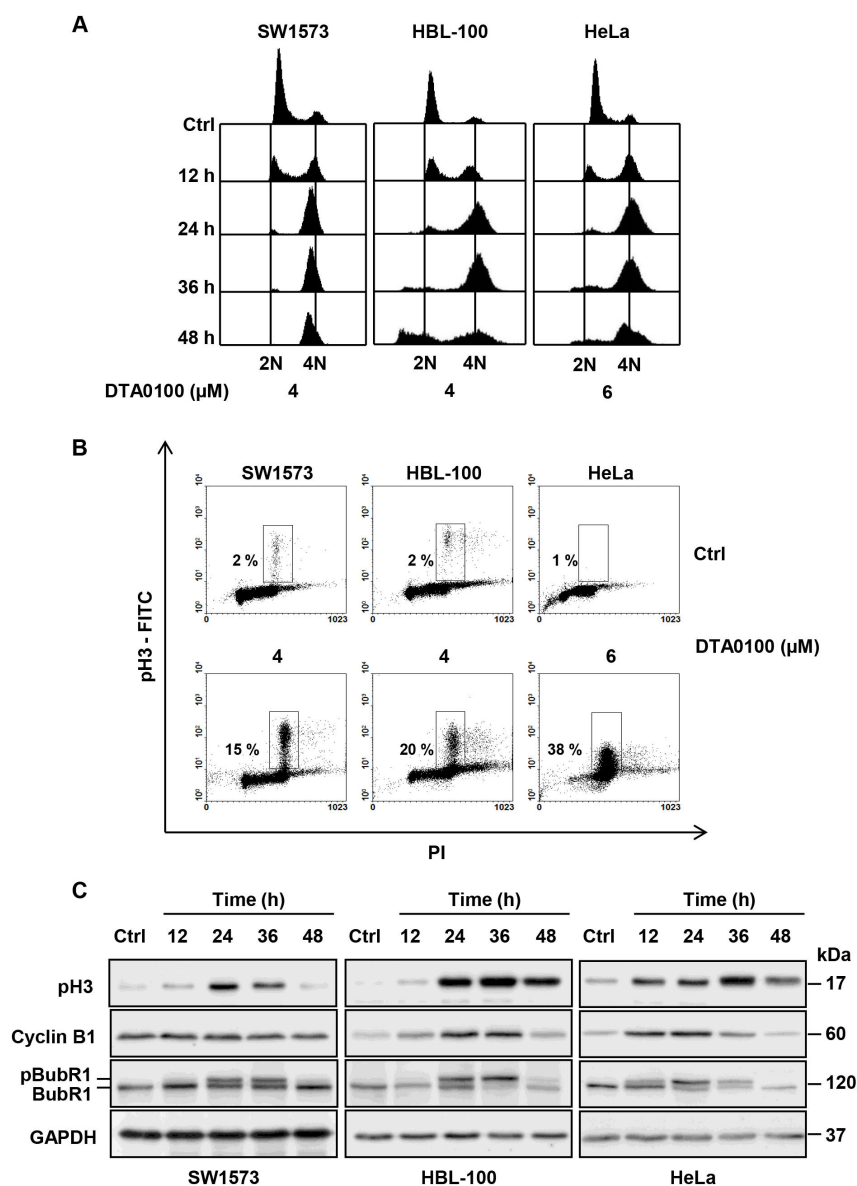


Fig. 2. (A) DTA0100 induces a G₂/M arrest in a time-dependent manner. Cell cycle histograms of untreated cells (control) and cells treated with DTA0100 for the indicated time. Cell cycle stage was determined by flow cytometric analysis of DNA content in individual cells. (B) DTA0100 inhibited cell growth and induced mitotic cell accumulation. Cells were treated with the indicated concentrations of DTA0100 for 24 h. Then, cell cycle stage was determined by flow cytometric analysis of DNA content and phosphohistone 3 (pH3) levels in individual cells. (C) DTA0100 specifically blocked cell cycle at mitosis. Cells were treated with 4 μM DTA0100 for the indicated time. Protein extracts were obtained for each condition and protein levels of pH3, cyclin B1, BubR1 and GAPDH were determined by western blotting.

3. Results

3.1. DTA0100 does not inhibit TOP2 activity in cells

To test whether or not DTA0100 (Fig. 1A) inhibits TOP2 activity in cells, nuclear extracts of SW1573 cells were used. We measured the supercoiled (SC) DNA relaxation activity of TOP2 in our nuclear preparations. Equal amounts of protein from nuclear extracts were incubated for 60 min with increasing concentrations of DTA0100 and resolved by 1% (w/v) agarose gel electrophoresis. For comparison, ellipticine, a catalytic inhibitor of TOP2, was used as a positive control. In the presence of DTA0100, TOP2 activity was not affected even at a high concentration as shown by the resolution of topoiso-

mers (Fig. 1B). On the other hand, TOP2 activity was completely inhibited by 100 μM ellipticine.

3.2. DTA0100 induces a mitotic delay with spindle assembly checkpoint activation

To determine the effect of DTA0100 on cell cycle progression, a time course experiment was performed. In all cell lines tested, DTA0100 induced a G₂/M arrest. This effect was observed after 24 h of treatment (Fig. 2A). In SW1573 cells, the G₂/M arrest was sustained throughout the experiment, with no evidence of cell death. However, in both HBL-100 and HeLa cells, PI staining profiles were also characterized by an increase in a sub-G₁ population within 36 h,

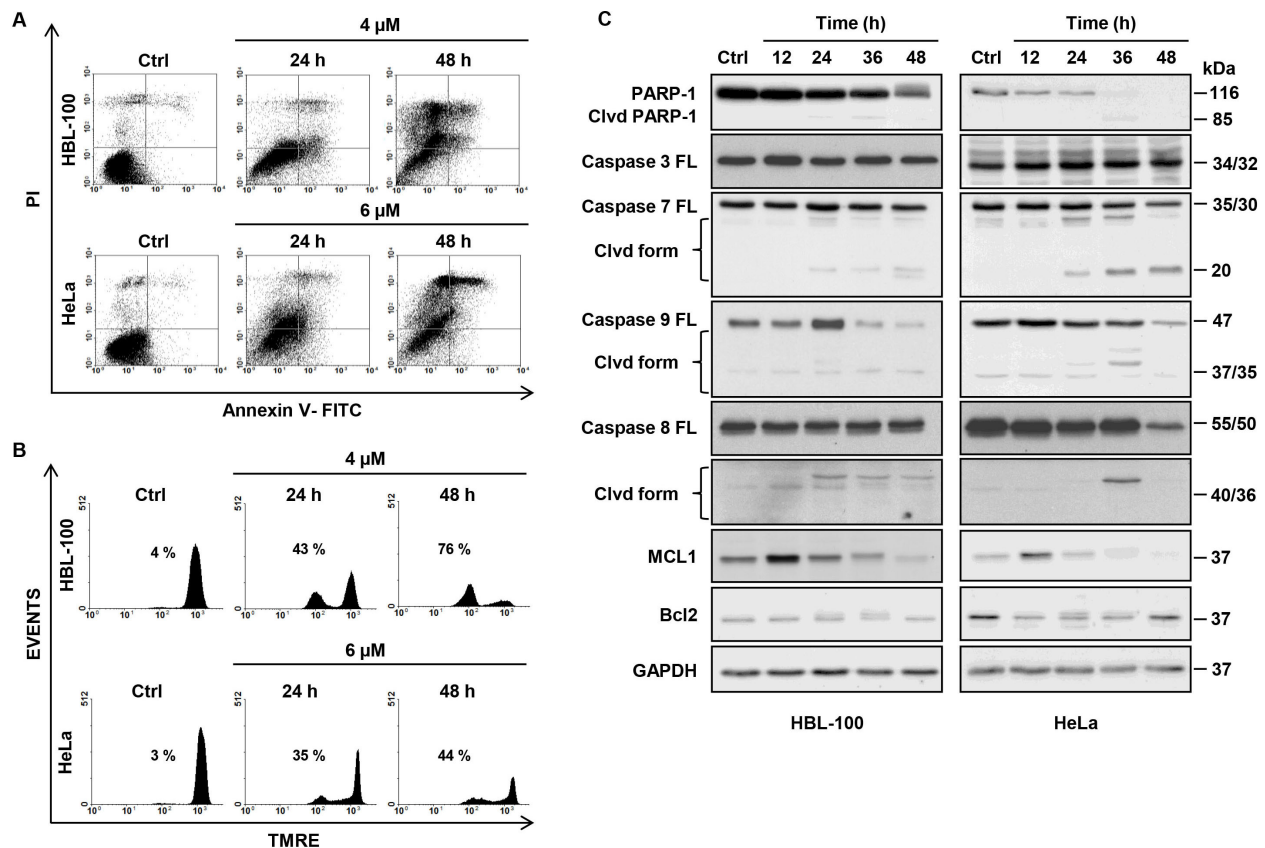


Fig. 3. (A) DTA0100 induces apoptotic cell death. HBL-100 and HeLa cells were treated at the indicated concentrations with DTA0100. After 24 h and 48 h of DTA0100 treatment, samples were taken and stained for annexin V-FITC and propidium iodide. (B) DTA0100 provoked MMP. HBL-100 and HeLa cells were treated with DTA0100 for the indicated times and $\Delta\Psi_m$ was evaluated using TMRE as a dye. Live single cells were gated and fluorescence intensity decrease of TMRE was quantified by flow cytometry. (C) DTA0100 caused cell death through a caspase-dependent mechanism. HBL-100 and HeLa cells were treated for the indicated times with DTA0100 and the expression of PARP, caspase 3, caspase 7, caspase 9 and caspase 8 were analyzed by western blotting. GAPDH was used as protein loading control.

an indicator of cell death.

During the above experiments, our attention was drawn that treatment with DTA0100 always caused the evident detachment of adherent tumor cells that became round, which was frequently observed during the mitosis phase. To test the possibility that DTA0100 could induce a specific mitotic arrest, we performed a flow cytometric analysis of positive cells for the phosphorylated form of histone 3 (Ser10), a mitotic-specific marker. We observed a shift from 1-5% for untreated cells to 12-34% for cells treated with DTA0100 for 24 h (Fig. 2B). This result confirmed a mitotic arrest induced by DTA0100.

Mitosis entrance was further confirmed by western blot analysis of mitotic markers as cyclin B1 and histone 3 (Fig. 2C). Moreover, treatment with DTA0100 resulted in attenuated phosphorylation of BubR1, which appeared as a characteristic, slower migrating band, that persisted for more than 24 h concomitant with a blockade in cell division in all treated cells, indicating a mitotic delay due to the activation of the spindle assembly checkpoint.

3.3. DTA0100 causes apoptosis through caspase activation

In addition to undergoing mitotic arrest, HBL-100 and HeLa treated cells also showed a sub- G_1 population upon cell cycle analysis. Therefore, we first assessed whether treatment with DTA0100

triggered apoptosis in these two cell lines. Annexin V staining showed an increase of apoptotic cells in a time-dependent manner in both cell lines compared with control cells (Fig. 3A). As the mitochondrial outer membrane becomes permeable during apoptosis, we asked if DTA0100 was able to induce changes in the mitochondrial membrane potential ($\Delta\Psi_m$). $\Delta\Psi_m$ was examined by the uptake of the TMRE dye (Fig. 3B). A decrease in TMRE fluorescence intensity was observed after 24 h of treatment in both cell lines. Next, we evaluated the biochemical parameters that are affected by apoptotic cell death. DTA0100 provoked PARP, caspase 7, caspase 9 and caspase 8 cleavages, with the generation of active fragments (Fig. 3C). The cleavage of these proteins occurred after 24 h of treatment in both cell lines. Surprisingly, no caspase 3 cleavage was observed under the same conditions, suggesting that DTA0100 was unable to activate caspase-3. This indicates that DTA0100 activates both the intrinsic and extrinsic apoptotic pathways.

Owing to the fact that mitochondrial membrane permeabilization is the central gate in turning on/off apoptosis, as it allows the release of a large panel of pro-apoptotic proteins, we evaluated the expression levels of some members of the Bcl-2 family. Western blot analysis revealed that DTA0100 reduced the mobility of anti-apoptotic Mcl-1 and Bcl-2 proteins suggesting a post-translational modification in both HBL-100 and HeLa cell lines at 24 h. After 36

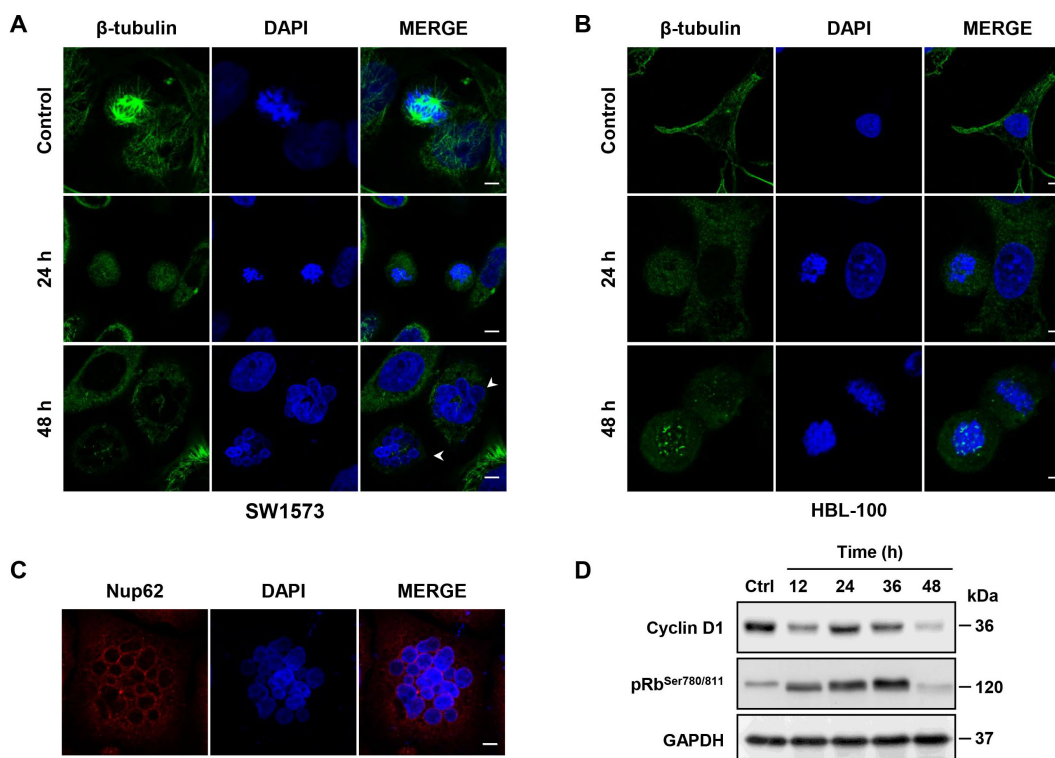


Fig. 4. DTA0100 disrupts the mitotic spindle. (A) SW1573 and (B) HBL-100 cells were treated with DTA0100 for 24 h and 48 h, fixed, stained with anti β -tubulin antibody (green) and counterstained with DAPI (blue). Representative confocal images of cellular preparations are shown. Scale bar: 10 μ m. (C) Induction of mitotic slippage by prolonged DTA0100 exposure in SW1573 cells. SW1573 cells were treated with DTA0100 for 48 h. Nuclear pore complex re-formation in cells upon mitotic slippage with the appearance of micronucleated cells in a tetraploid G_0 -state. Scale bar: 10 μ m. (D) Tetraploid G_0 arrest induced by DTA0100. Western blot analysis of cyclin D1, pRb^{Ser780/811}, p53 and p21. Cytoplasmic GAPDH was used as loading control.

h, the majority of Mcl-1 had disappeared and was almost completely absent at 48 h for both cell lines. Meanwhile, the modified state of Bcl-2 remained until 36 h of treatment (Fig. 3C).

3.4. DTA0100 disrupts the mitotic spindle

We stained DTA0100-treated cells for tubulin by immunofluorescence whereas chromosomes were stained with DAPI. Control cells in the interphase exhibited normal fine filamentous arrays of microtubules and mitotic cells had well-organized bipolar spindles with compact metaphase plates of condensed chromosomes (Fig. 4A, 4B). Treatment with DTA0100 for 24 h caused a strong diffused green staining typical for depolymerized tubulins in all cell lines. Nuclear staining showed condensed DNA with irregular structure confirming that cells were arrested in prometaphase. The same effect was observed at 48 h. However, in SW1573 cells DTA0100 induced the formation of multinucleated interphase cells.

Hyperploid formation in SW1573 cells after DTA0100 exposure suggested that cells were presumably able to adapt, escape from mitotic arrest and enter into a tetraploid G_1 state without cell division, a phenomenon defined as mitotic slippage. To test this effect, we first examined the presence of nucleoporin 62 (Nup62) ring after 24 and 48 h of treatment (Fig. 4C). As compared with control cells, at 24 h, cells lacked Nup62 rings and exhibited chromosomal condensation, which is characteristic of morphological changes seen in cells blocked in mitotic prometaphase. By 48 h, most cells had reconstituted Nup62 ring and the appearance of giant micronucleated cells and uncondensed chromatin was observed. Tetraploid G_1 state was

confirmed with the expression of putative G_0/G_1 cell cycle markers, cyclin D1 and the hyperphosphorylated form of Rb (pRb). In our immunoblotting experiments (Fig. 4D), we found increased levels of cyclin D1 and hyperphosphorylated pRb at 24 h. Strikingly, after 48 h of DTA0100 exposure, cyclin D1 and hyperphosphorylated pRb were undetectable. Thus, the status of the proteins bore similarity to the G_0 hallmark found in confluent cells.

3.5. DTA0100 inhibits microtubule polymerization

Due to the observed effect on microtubules, we thus wondered if DTA0100 had a direct effect on microtubule polymerization. We used two in vitro microtubule polymerization assays. For the microtubule-pull down experiments 20 μ M colchicine and paclitaxel were used as depolymerization and polymerization controls, respectively. We found that colchicine and DTA0100 (20 μ M) prevented microtubule polymerization as indicated by the prevalence of soluble tubulin (Fig. 5A). In contrast, tubulin treated with paclitaxel was polymerized. To better quantify how DTA0100 affects tubulin polymerization, we monitored tubulin polymerization by following the absorbance of the solution at 340 nm for 30 min. An increase in absorbance indicated an increase in tubulin polymerization. In this experiment, we included nocodazole as depolymerization control. All the compounds were tested at the same concentration (10 μ M) for comparison purposes. As expected, paclitaxel increased the absorbance above the control while colchicine, nocodazole and DTA0100 strongly inhibited microtubule polymerization (Fig. 5B).

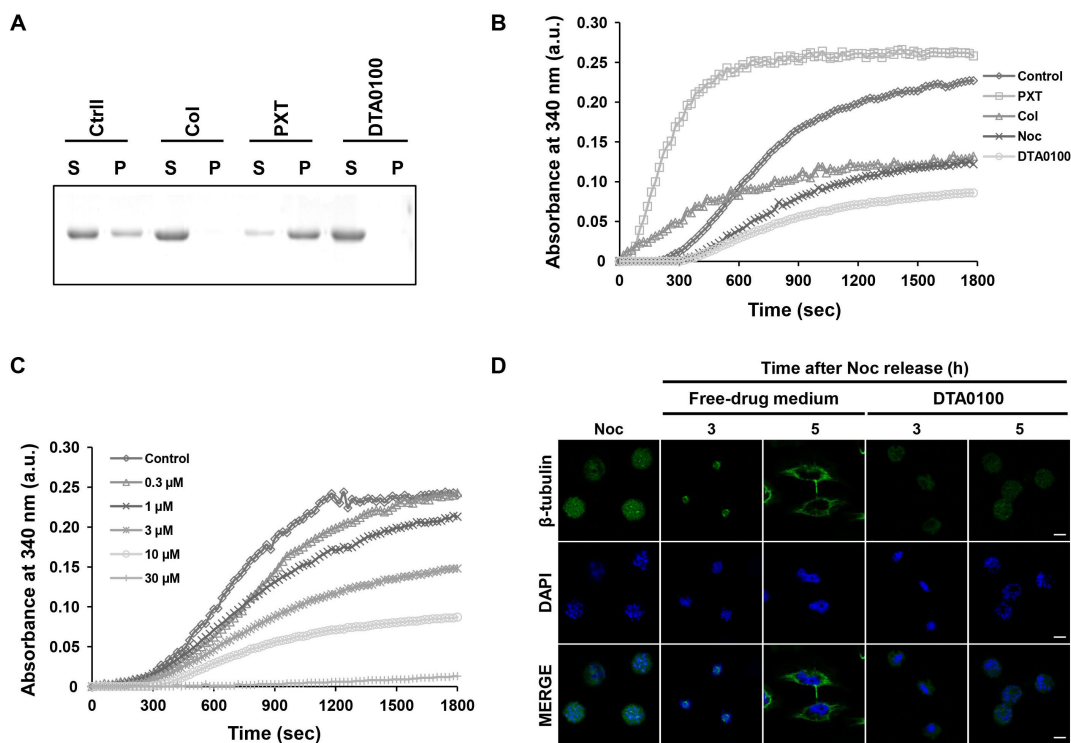


Fig. 5. DTA0100 inhibits microtubule polymerization in a dose-dependent manner. (A) Tubulin was polymerized for 30 min at 37°C in the presence of 20 μ M of the indicated compounds. Colchicine (Col) and paclitaxel (PXT) were used as controls. After ultracentrifugation, the supernatant (S) and pellet (P) were analyzed by SDS-PAGE and stained with Coomassie. (B) Tubulin was polymerized for 30 min at 37 °C in the presence of 10 μ M of the indicated molecules, including nocodazole (NOC) and the absorbance at 340 nm was measured. (C) Tubulin was polymerized for 30 min at 37°C in the presence of different concentrations of DTA0100. (D) DTA0100 impeded NOC-arrested cells recovery. After nocodazole treatment, cells were released in fresh medium with and without DTA0100 for the indicated period of times. Cells were fixed, stained with β -tubulin antibody (green) and counterstained with DAPI (blue). Representative confocal images for cellular preparations are shown. Scale bar 10 μ m.

DTA0100 destabilized microtubules in a dose-dependent manner, as seen in Fig. 5C.

To further verify that DTA0100 behaved as a typical depolymerization agent and blocks tubulin polymerization in cells, we assessed the ability of DTA0100 to impede mitotic spindle reorganization after disassembly induced by nocodazole. SW1573 cells were treated with nocodazole for 20 h. Then, nocodazole was washed out and cells were released in fresh medium with and without DTA0100. As shown in Fig. 5D, nocodazole treatment resulted in complete dissolution of mitotic spindle. When nocodazole was removed and cells were released in fresh medium, we observed the formation of mitotic spindles within 3 h suggesting that the cells were recovering from the arrest. Five hours later, the majority of cells exited mitosis. In contrast, cells exposed to DTA0100 after release, remained arrested in mitosis with no evidence of mitotic spindle repolymerization. This result suggested that DTA0100 had a direct effect on tubulin polymerization, hence blocking reassembly of microtubules after nocodazole release with preferential affinity for tubulin heterodimers.

3.6. DTA0100 binds to tubulin at the colchicine-binding site

Microtubule-destabilizing agents often have specific microtubule binding sites. In order to define DTA0100 binding site, we performed a competition experiment in the presence of MTC, an analog of colchicine. Using a spectrofluorometric assay, DTA0100 was assayed for its ability to displace MTC from its binding at the colchicine

site. As evident from Fig. 6A, the fluorescence of MTC-tubulin complex was decreased with increasing concentrations of DTA0100. At 12.5 μ M, the fluorescence level was reduced by 25%. At 100 μ M, DTA0100 reduced the fluorescence to 40% and at 200 μ M to 56%. When compared to colchicine (Fig. 6B), over 50% of the fluorescence level was reduced at 25 μ M. In contrast, no changes in fluorescence levels were observed when vinblastine was added even at high doses (data not shown), and the small fluorescence decrease observed could be non-specific. These data showed that DTA0100 was able to compete with MTC for the colchicine binding domain.

To gain further insight into the tubulin binding site of DTA0100, computation-based docking analysis was performed for the colchicine binding domain. This was performed while taking into account that DTA0100 is a racemic mixture, and the docking protocol was extended to both DTA0100 enantiomers. This analysis revealed that both enantiomers bound well at the colchicine binding domain of β -tubulin, with good Gibbs free energy (Δ G) values. Regarding (R)-DTA0100, the docking model showed a potential H-bond formed with Tyr202 and the carbonyl of the alkyne end, while two other interactions were found between Val238 and Lys254 with the methoxy group of the alkyne end and the methoxy group of the enol ether, respectively (Fig. 7A). For (S)-DTA0100, Tyr202 underwent a hydrogen bonding interaction with the oxygen atom of the carbonyl of the enol ether. We also observed interactions between Val238 and Lys254 and the two methoxy groups of the molecule (Fig. 7B). These docking results showed that chirality is not a limiting factor

Table 1. Anti-proliferative activity (GI_{50}) of DTA100 and tubulin-interacting drugs in SW1573 and SW1573/P-gp cell lines^a

	– Verapamil			+ Verapamil		
	SW1573	SW1573/P-gp	Rf ^b	SW1573	SW1573/P-gp	Rf
DTA0100	1029 ± 221	2902 ± 476	3	656 ± 252	2637 ± 713	4
Paclitaxel	1.5 ± 0.5	196 ± 53	128	1.6 ± 0.2	4.2 ± 0.9	3
Colchicine	71 ± 15	531 ± 95	7	46 ± 11	131 ± 7	3
Vincristine	9.7 ± 3.6	180 ± 68	18	1.5 ± 0.3	3.8 ± 0.5	3
Vinblastine	0.9 ± 0.3	2051 ± 682	2388	0.8 ± 0.2	1.0 ± 0.5	1

^aValues are given in nM and represent mean values of at least three independent experiments ± standard deviation.

^bRf represents the ratio between GI_{50} SW1573/P-gp and SW1573.

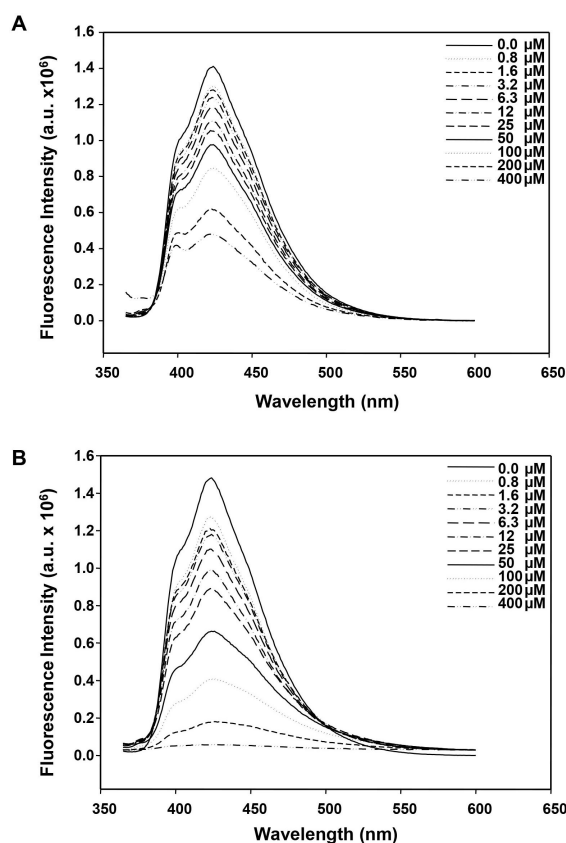


Fig. 6. Displacement of MTC from the colchicine binding domain by DTA0100. Fluorescence emission spectra of MTC-tubulin complex co-incubated with different concentrations of (A) DTA0100 and (B) colchicine in 10 mM sodium phosphate buffer pH 7.0 containing 0.1 mM GTP at 25°C.

for the activity of DTA0100, and revealed how DTA0100 binds to the colchicine binding domain. These studies are the starting point of the lead optimization process that will allow us to improve the biological activity of DTA0100.

3.7. P-gp does not affect the activity of DTA0100

To determine whether or not P-gp could affect the activity of DTA0100, we determined the GI_{50} values after 48 h of exposure to DTA0100 in wild type and P-gp overexpressing SW1573 cells, and in the presence of the P-gp transport inhibitor verapamil (at a fixed concentration of 10 μ M). The standard microtubule-interacting

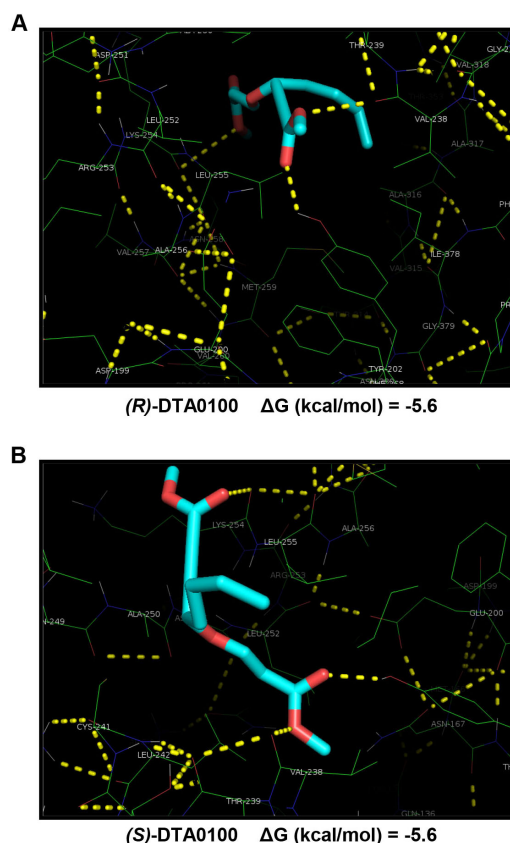


Fig. 7. Comparison of R-DTA0100 and S-DTA0100 conformations at the colchicine binding domain of tubulin. Localization of docked configurations of ligands are primarily in β -tubulin. (A) R-DTA0100 and (B) S-DTA0100. Residues thought to interact with the compounds are represented as thin dashed lines. Compounds are shown in stick representation.

drugs colchicine, vincristine, vinblastine and paclitaxel were used for comparison purposes. Table 1 shows the GI_{50} values obtained after 48 h of drug exposure. For better comparison of the data, we defined resistance factor (Rf) for a given compound as the ratio of GI_{50} values against the P-gp overexpressing and the wild-type cell lines, respectively. In the absence of verapamil, we observed that DTA0100 was the least affected compound by P-gp overexpression (Rf = 4). In contrast, vinblastine was the most affected compound (Rf = 2388). Co-treatment with verapamil produced a decrease in Rf for all anti-mitotic drugs tested. However, for DTA0100, the Rf

value remained constant. These results indicate that the activity of DTA0100 is not affected by the overexpression of P-gp.

4. Discussion

This study was carried out in a stepwise fashion and was accomplished in sequential stages according to previously obtained results. In general, the framework of our Phenotypic Drug Discovery (PDD) approach comprises four well-defined steps, so-called Anti-proliferative (or Primary), Secondary, Target and Confirmatory assays. Herein, we proposed a strategy that could be applied to any given small molecule from diverse origins: either natural, semi-synthetic or synthetic. We exemplified our PDD approach by establishing a methodology aimed to uncover the mechanism of action of new propargylic enol ether derivatives obtained by a catalytic multicomponent domino process [9]. The same approach might aid to discard targets without the need of testing them individually [1]. The combination of phenotypic data with computational methods represents another alternative that we have explored with success [3].

The lead compound DTA0100, was selected from a small and structure-focused library of 30 analogs. DTA0100 induces mitotic arrest in human cancer cell lines and was found to act as a TOP2 catalytic inhibitor [2]. In addition, its inhibitory activity was not affected by the stereochemistry of the chiral center [10]. However, when the fluorescent analog (dns-DTA0100) was used to study the subcellular localization, no staining was observed in the nucleus. This result suggested that TOP2 was presumably not the main molecular target of DTA0100 inside the cells [4]. In addition, DTA0100 failed to inhibit the TOP2 activity of nuclear extracts isolated from SW1573 cells. Collectively, these two outcomes revealed no compelling evidence for a direct inhibition of TOP2 in cells by DTA0100. These results forced us to rethink about the presence of alternative cellular targets. Therefore, we conducted new experiments in order to understand the mechanism of action of DTA0100.

After a prolonged mitotic arrest, cells have three possible fates. First, cells may eventually complete cell division after a mitotic delay [11]. Such divisions frequently precede mis-segregation of chromosomes, thereby leading to aneuploidy. Second, cells can undergo mitotic slippage, a process whereby mitotic cells return to interphase without completing anaphase [12]. In this case, since cell division does not occur, the resulting interphase cells, which are often referred to as post-mitotic, will possess twice the normal number of chromosomes with a nucleus that tends to consist of multiple micronuclei, making them tetraploid. After either of these first two fates, cells will then realize one of three additional fates: continuation of the cell cycle, cell death, or cell cycle arrest. Finally, a third fate following prolonged checkpoint activation is mitotic cell death, where cells die directly from the mitotic state [13]. Time-course experiments demonstrated a mitotic arrest in each cell line tested with different phenotypic patterns depending on the cell line. Thus, DTA0100 triggers apoptosis of HBL-100 and HeLa cells as a consequence of the prolonged mitotic arrest. In contrast, SW1573-treated cells were able to overcome mitotic delay and were arrested in a G₀-like state that prevented cells to re-replicate in a DNA damage-independent p53-mediated tetraploid checkpoint. The activation of this checkpoint did not require the entrance of cells into the cell cycle.

It was clear that DTA0100 affects the mitotic machinery. To better characterize its effect in mitosis, perturbations of mitotic spin-

dle and chromosome segregation were examined in all cell lines. The results pointed to a block in mitotic prometaphase, which was associated with depolymerization of tubulin. Anti-tubulin agents are divided into two categories, microtubule stabilizers and destabilizers, based on their ability to bind to tubulin and change the ratio between assembled microtubules and dimeric tubulin [14]. Three classic binding sites for small anti-tubulin agents are known and are responsible for the interactions and pharmacological effects of paclitaxel, vinblastine, and colchicine [15]. Paclitaxel, a classic microtubule stabilizing agent preferably binds to polymeric tubulin as opposed to its dimeric form. Vinblastine and colchicine, microtubule destabilizing agents, preferentially bind to heterodimeric tubulin. Vinblastine binds to the β -tubulin subunit distinct region known as Vinca-binding domain, while colchicine binds to the β -subunit at the interface with α -monomer of the same tubulin molecule. Specific experiments suggested that DTA0100 had a direct effect on tubulin polymerization, blocking reassembly of microtubules after nocodazole release with preferential affinity for tubulin heterodimers. Furthermore, DTA0100 was found to target the colchicine-binding domain and computational studies indicated similar binding modes for both enantiomers with good Gibbs free energy values of -5.6 kcal/mol. They also showed no interactions with the α -subunit.

Drug resistance remains a challenge in the treatment of various diseases, especially in cancer. Tubulin targeting agents are known to be antagonized by the P-gp drug-efflux pump. Thus, compounds that can both tackle microtubules and evade recognition by P-gp remain unmet medical needs [16, 17]. In this context, DTA0100 behaved as a non-P-gp substrate and appears to be a good candidate to overcome multidrug resistance [4].

5. Conclusion

In conclusion, we propose a strategy based on a PDD approach that can address the mechanism of action at early stages of drug discovery. Our strategy relies on the use of a set of biological experiments organized in a modular fashion. The rational use of chemical techniques in synergy with biological methods in this study led us to understand the bioactivity, at the cellular level, of a lead compound selected from a small library of compounds. Moreover, both areas are the foundation that provides a robust and reliable methodology for the identification of target candidates. In this context, bioactive small molecules can be discovered effectively by using a modular approach based on phenotypic changes induced by new chemical entities.

Acknowledgements

Co-financed by the EU Research Potential (FP7-REGPOT-2012-CT2012-31637-IMBRAIN), the European Regional Development Fund (FEDER), and the Spanish Instituto de Salud Carlos III (PI11/00840).

Conflict of Interest

All the authors declare no conflicts of interest.

References

- [1] Rios-Luci C, Dominguez-Kelly R, Leon LG, Diaz-Rodriguez E, Freire R, Pandiella A, *et al.* A modular approach to trim cellular targets in anticancer drug discovery. *Bioorg Med Chem Lett*, 2011; 21(22): 6641-5.

- [2] Leon LG, Rios-Luci C, Tejedor D, Perez-Roth E, Montero JC, Pandiella A, *et al.* Mitotic arrest induced by a novel family of DNA topoisomerase II inhibitors. *J Med Chem*, 2010; 53(9): 3835-9.
- [3] Silveira-Dorta G, Sousa IJ, Fernandes MX, Martín VS, Padrón JM. Synthesis and identification of unprecedented selective inhibitors of CK1 ϵ . *Eur J Med Chem*, 2015; 96: 308-17.
- [4] Podolski-Renic A, Bankovic J, Dinic J, Rios-Luci C, Fernandes MX, Ortega N, *et al.* DTA0100, dual topoisomerase II and microtubule inhibitor, evades paclitaxel resistance in P-glycoprotein overexpressing cancer cells. *Eur J Pharm Sci*, 2017; 105: 159-68.
- [5] Kepp O, Galluzzi L, Lipinski M, Yuan J, Kroemer G. Cell death assays for drug discovery. *Nat Rev Drug Discov*, 2011; 10(3): 221-37.
- [6] Bradford MM. A rapid and sensitive method for the quantitation of microgram quantities of protein utilizing the principle of protein-dye binding. *Anal Biochem*, 1976; 72: 248-54.
- [7] Palmeira A, Vasconcelos MH, Paiva A, Fernandes MX, Pinto M, Sousa E. Dual inhibitors of P-glycoprotein and tumor cell growth: (re)discovering thioxanthenes. *Biochem Pharmacol*, 2012; 83(1): 57-68.
- [8] Castillo QA, Triana J, Eiroa JL, Calcul L, Rivera E, Wojtas L, *et al.* ent-Labdane diterpenoids from the aerial parts of *Eupatorium obtusissimum*. *J Nat Prod*, 2016; 79(4): 907-13.
- [9] Tejedor D, Gonzalez-Cruz D, Santos-Exposito A, Marrero-Tellado JJ, De Armas P, Garcia-Tellado F. Multicomponent domino processes based on the organocatalytic generation of conjugated acetylides: efficient synthetic manifolds for diversity-oriented molecular construction. *Chemistry*, 2005; 11(12): 3502-10.
- [10] Silveira-Dorta G, Sousa IJ, Ríos-Luci C, Martín VS, Fernandes MX, Padrón JM. Molecular docking studies of the interaction between propargylic enol ethers and human DNA topoisomerase II α . *Bioorg Med Chem Lett*, 2013; 23(19): 5382-4.
- [11] Gascoigne KE and Taylor SS. Cancer cells display profound intra- and interline variation following prolonged exposure to antimetabolic drugs. *Cancer Cell*, 2008; 14(2): 111-22.
- [12] Rieder CL and Maiato H. Stuck in division or passing through: what happens when cells cannot satisfy the spindle assembly checkpoint. *Dev Cell*, 2004; 7(5): 637-51.
- [13] Dalton WB and Yang VW. Role of prolonged mitotic checkpoint activation in the formation and treatment of cancer. *Future Oncol*, 2009; 5(9): 1363-70.
- [14] Li CM, Lu Y, Ahn S, Narayanan R, Miller DD, Dalton JT. Competitive mass spectrometry binding assay for characterization of three binding sites of tubulin. *J Mass Spectrom*, 2010; 45(10): 1160-6.
- [15] Gireesh KK, Rashid A, Chakraborti S, Panda D, Manna T. CIL-102 binds to tubulin at colchicine binding site and triggers apoptosis in MCF-7 cells by inducing monopolar and multinucleated cells. *Biochem Pharmacol*, 2012; 84(5): 633-45.
- [16] Nguyen TL, Cera MR, Pinto A, Lo Presti L, Hamel E, Conti P, *et al.* Evading Pgp activity in drug-resistant cancer cells: a structural and functional study of antitubulin furan metocic compounds. *Mol Cancer Ther*, 2012; 11(5): 1103-11.
- [17] Stark M and Assaraf YG. Structural recognition of tubulysin B derivatives by multidrug resistance efflux transporters in human cancer cells. *Oncotarget*, 2017; 8(30): 49973-87.